nature medicine

LETTERS

Intrinsic BET inhibitor resistance in *SPOP*-mutated prostate cancer is mediated by BET protein stabilization and AKT–mTORC1 activation

Pingzhao Zhang[1,2,13], Dejie Wang[3–5,13], Yu Zhao[3,13], Shancheng Ren[6,13], Kun Gao[1,13], Zhenqing Ye[7], Shangqian Wang[8], Chun-Wu Pan[3], Yasheng Zhu[6], Yuqian Yan[3], Yinhui Yang[3], Di Wu[3], Yundong He[3], Jun Zhang[9], Daru Lu[1], Xiuping Liu[10], Long Yu[1], Shimin Zhao[1], Yao Li[1], Dong Lin[11], Yuzhuo Wang[11], Liguo Wang[7], Yu Chen[8], Yinghao Sun[6], Chenji Wang[1] & Haojie Huang[3,5,12]

Bromodomain and extraterminal domain (BET) protein inhibitors are emerging as promising anticancer therapies. The gene encoding the E3 ubiquitin ligase substrate-binding adaptor speckle-type POZ protein (SPOP) is the most frequently mutated in primary prostate cancer. Here we demonstrate that wild-type SPOP binds to and induces ubiquitination and proteasomal degradation of BET proteins (BRD2, BRD3 and BRD4) by recognizing a degron motif common among them. In contrast, prostate cancer–associated SPOP mutants show impaired binding to BET proteins, resulting in decreased proteasomal degradation and accumulation of these proteins in prostate cancer cell lines and patient specimens and causing resistance to BET inhibitors. Transcriptome and BRD4 cistrome analyses reveal enhanced expression of the GTPase *RAC1* and cholesterol-biosynthesis-associated genes together with activation of AKT–mTORC1 signaling as a consequence of BRD4 stabilization. Our data show that resistance to BET inhibitors in *SPOP*-mutant prostate cancer can be overcome by combination with AKT inhibitors and further support the evaluation of *SPOP* mutations as biomarkers to guide BET-inhibitor-oriented therapy in patients with prostate cancer.

Ubiquitously expressed BET proteins, including BRD2, BRD3 and BRD4, function as key factors in transcriptional activation of distinct sets of cancer-related genes through context-specific interaction with acetylated histones and/or transcription factors[1,2]. Several small-molecule inhibitors specifically targeting the bromodomains of BET proteins have been developed and display promising anticancer activity via selective blockade of expression of cancer promoters, such as MYC in multiple myeloma and androgen receptor (AR) in prostate cancer[1–6]. Although BET inhibitors are undergoing clinical trials as treatment for various cancer types, several mechanisms of drug resistance have been documented[7–9]. At present, there are no genetic alterations that can be exploited as biomarkers to guide targeted use of these drugs.

SPOP is the substrate-recognition subunit of the cullin-3 (CUL3)–RING-box 1 (RBX1) E3 ubiquitin ligase (CRL) complex. SPOP binding triggers the ubiquitination and proteasomal degradation of target proteins mediated by RBX1-dependent recruitment of E2 ubiquitin-conjugating enzyme into the CRL complex. Cancer whole-genome and exome sequencing studies have shown that *SPOP* is the most frequently mutated gene in primary prostate cancer[10,11]. Notably, *SPOP* mutations detected in prostate cancer map to the structurally defined substrate-binding motif termed the meprin and TRAF homology (MATH) domain[10,12–14], suggesting that the pathophysiology resulting from *SPOP* mutations is likely mediated by impaired ubiquitination of substrates.

To identify new degradation substrates of SPOP, we performed yeast two-hybrid screens using full-length SPOP as bait. A total of 246 SPOP-interacting clones were obtained, including ones in which the known SPOP substrates DEK and steroid receptor coactivator 3 (SRC-3) were prey (**Supplementary Table 1**). Gene ontology analysis showed that SPOP bound to a number of proteins involved in regulation

[1]State Key Laboratory of Genetic Engineering, Collaborative Innovation Center for Genetics and Development, School of Life Sciences, Fudan University, Shanghai, China. [2]Fudan University Shanghai Cancer Center and Institute of Biomedical Sciences, Shanghai Medical College, Fudan University, Shanghai, China. [3]Department of Urology, Mayo Clinic College of Medicine, Rochester, Minnesota, USA. [4]Department of Gastroenterology, Jiangxi Institute of Gastroenterology and Hepatology, First Affiliated Hospital of Nanchang University, Nanchang, China. [5]Department of Biochemistry and Molecular Biology, Mayo Clinic College of Medicine, Rochester, Minnesota, USA. [6]Department of Urology, Shanghai Changhai Hospital, Second Military Medical University, Shanghai, China. [7]Division of Biomedical Statistics and Informatics, Mayo Clinic College of Medicine, Rochester, Minnesota, USA. [8]Human Oncology and Pathogenesis Program, Memorial Sloan Kettering Cancer Center, New York, New York, USA. [9]Department of Laboratory Medicine and Pathology, Mayo Clinic College of Medicine, Rochester, Minnesota, USA. [10]Department of Pathology, School of Basic Medical Sciences, Shanghai Medical College of Fudan University, Shanghai, China. [11]Department of Experimental Therapeutics, BC Cancer Research Centre, Vancouver, British Columbia, Canada. [12]Mayo Clinic Cancer Center, Mayo Clinic College of Medicine, Rochester, Minnesota, USA. [13]These authors contributed equally to this work. Correspondence should be addressed to H.H. (huang.haojie@mayo.edu), C.W. (chenjiwang@fudan.edu.cn) or Y.S. (sunyhsmmu@126.com).

Received 2 June; accepted 29 June; published online 14 August 2017; doi:10.1038/nm.4379

of various signaling pathways, but the top hit was the BET proteins (**Fig. 1a** and **Supplementary Table 2**). Coimmunoprecipitation (co-IP) assays confirmed that ectopically expressed and endogenous SPOP interacted with BRD2, BRD3 and BRD4 in 293T and LNCaP prostate cancer cells (**Fig. 1b** and **Supplementary Fig. 1a**). Thus, SPOP interacts with BET proteins in physiological conditions.

BET proteins play key roles in epigenetic regulation and cancer, but little is known about their post-translational modifications and downstream functions. Treatment of LNCaP cells with the proteasome inhibitors bortezomib and MG-132 inevitably increased BET protein levels but not corresponding mRNA levels (**Supplementary Fig. 1b**,**c**). MLN4924, a small-molecule inhibitor of NEDD8-activating enzyme that is required for activation of CRL complexes, also caused accumulation of BET proteins (**Supplementary Fig. 1b**,**c**). Expression of wild-type SPOP markedly decreased BET protein levels in comparison to cells transfected with empty vector, and this effect was completely reversed by MG-132 treatment (**Fig. 1c**). Relative to control knockdown, SPOP knockdown increased the steady-state levels of endogenous BET proteins and prolonged protein half-life but had no overt effect on corresponding mRNA levels in LNCaP cells (**Fig. 1d** and **Supplementary Fig. 1d**–**f**). Similar results were obtained in the 22Rv1 and BPH-1 prostate cell lines (**Fig. 1d**). Moreover, only wild-type SPOP—and not substrate-binding- and CUL3-binding-deficient mutants (with deletion of the MATH domain (ΔMATH) and deletion of the BTB domain (ΔBTB), respectively)—degraded BET proteins (**Supplementary Fig. 1g**). Expression of wild-type SPOP induced K48-dependent polyubiquitination of these proteins in cells, and this effect relied on the enzymatic activity of SPOP (**Fig. 1e** and **Supplementary Fig. 1h**,**i**). We further found that the SPOP–CUL3–RBX1 complex catalyzed BRD4 ubiquitination *in vitro* (**Fig. 1f**). Thus, functioning as a CRL substrate-binding adaptor, SPOP promotes ubiquitination and proteasomal degradation of BET proteins in prostate cancer cells.

Substrate-binding consensus (SBC) motifs (Φ-π-S/T-S/T-S/T, where Φ is a nonpolar residue and π is a polar residue[15]) have been well characterized in known SPOP substrates, such as macroH2A and DEK[12]. We found a perfectly matched SBC motif in the region between bromodomain-1 (BD1) and BD2 in each BET protein (**Fig. 2a**,**b**), which was also located within the minimal SPOP-interaction region defined by yeast two-hybrid clones (**Fig. 1a**). Co-IP assays revealed that deletion of the putative SBC motif in the BET proteins not only abolished SPOP binding and SPOP-mediated ubiquitination and degradation of these proteins, but also substantially prolonged their half-lives in 293T cells (**Fig. 2b**–**g**). Thus, we identified a shared, functionally conserved SBC motif in BET proteins that is required for SPOP-dependent ubiquitination and degradation.

Because *SPOP* mutations in prostate cancers map to the MATH domain, which is responsible for substrate binding[16], we hypothesized that prostate cancer–associated mutations impair the ability of SPOP to degrade BET proteins. Eleven prostate cancer–associated SPOP mutants were generated and expressed in 293T cells. Co-IP assays demonstrated that the BET-protein-binding ability of all 11 SPOP mutants was greatly impaired in comparison with that of wild-type SPOP (**Fig. 3a** and **Supplementary Fig. 2a**). SPOP-mediated ubiquitination of the BET proteins was also markedly attenuated for these mutants (**Fig. 3b** and **Supplementary Fig. 2b**). SPOP mutants failed to degrade BET proteins and instead led to elevated endogenous levels of BRD2, BRD3 and BRD4, showing a dominant-negative effect similar to that occurring with confirmed SPOP substrates such as DEK, ERG and SRC-3 (refs. 12–14) (**Fig. 3c**). Thus, prostate

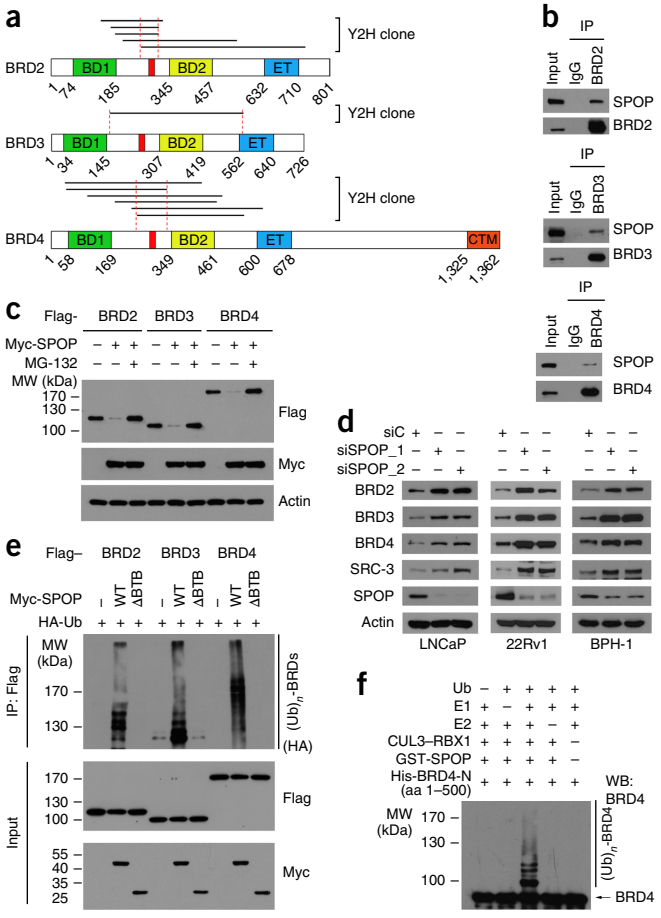

Figure 1 SPOP interacts with and promotes BET protein ubiquitination and degradation. (**a**) Diagram showing the portions of the BRD2, BRD3 and BRD4 proteins identified by yeast two-hybrid (Y2H) screen in a human fetal brain cDNA library using full-length SPOP as bait. The region between each pair of dashed red lines is the minimal interaction region shared by positive clones, and the red rectangles represent the SBC motif. BD1, bromodomain-1; BD2, bromodomain-2; ET, extraterminal domain; CTM, C-terminal motif. (**b**) Western blots of samples from co-IP analysis using IgG or anti-BRD2, anti-BRD3 or anti-BRD4 antibody on cell lysate from LNCaP cells treated with 20 μM MG-132 for 8 h. (**c**) Western blots of whole-cell lysate (WCL) from 293T cells transfected with the indicated constructs and treated with 20 μM MG-132 or left untreated for 8 h. Actin was used as a loading control. MW, molecular weight. (**d**) Western blots of the WCL of different cell lines transfected with the indicated small interfering RNAs (siRNAs). siC, control siRNA. (**e**) Western blots of the products of *in vivo* ubiquitination assays performed using cell lysate from 293T cells transfected with the indicated constructs and treated with 20 μM MG-132 for 8 h. WT, wild type; Ub, ubiquitin. (**f**) Western blot (WB) of the products of *in vitro* ubiquitination assays performed by incubating the reconstituted SPOP–CUL3–RBX1 E3 ligase complex with E1 and E2 enzymes, ubiquitin and His-BRD4-N (amino acids 1–500) at 30 °C for 2 h.

cancer–associated *SPOP* mutations result in the stabilization of BET proteins in prostate cancer cells.

To examine the effect of *SPOP* mutations on BET protein levels in specimens from individuals with prostate cancer, we analyzed BRD2, BRD3 and BRD4 protein levels in two cohorts for which a total of 99 primary prostate tumor samples were available (**Supplementary Table 3**). We identified 13 *SPOP*-mutated tumors through whole-genome sequencing and/or Sanger sequencing. The *SPOP* mutation frequency in our samples is consistent with previous findings

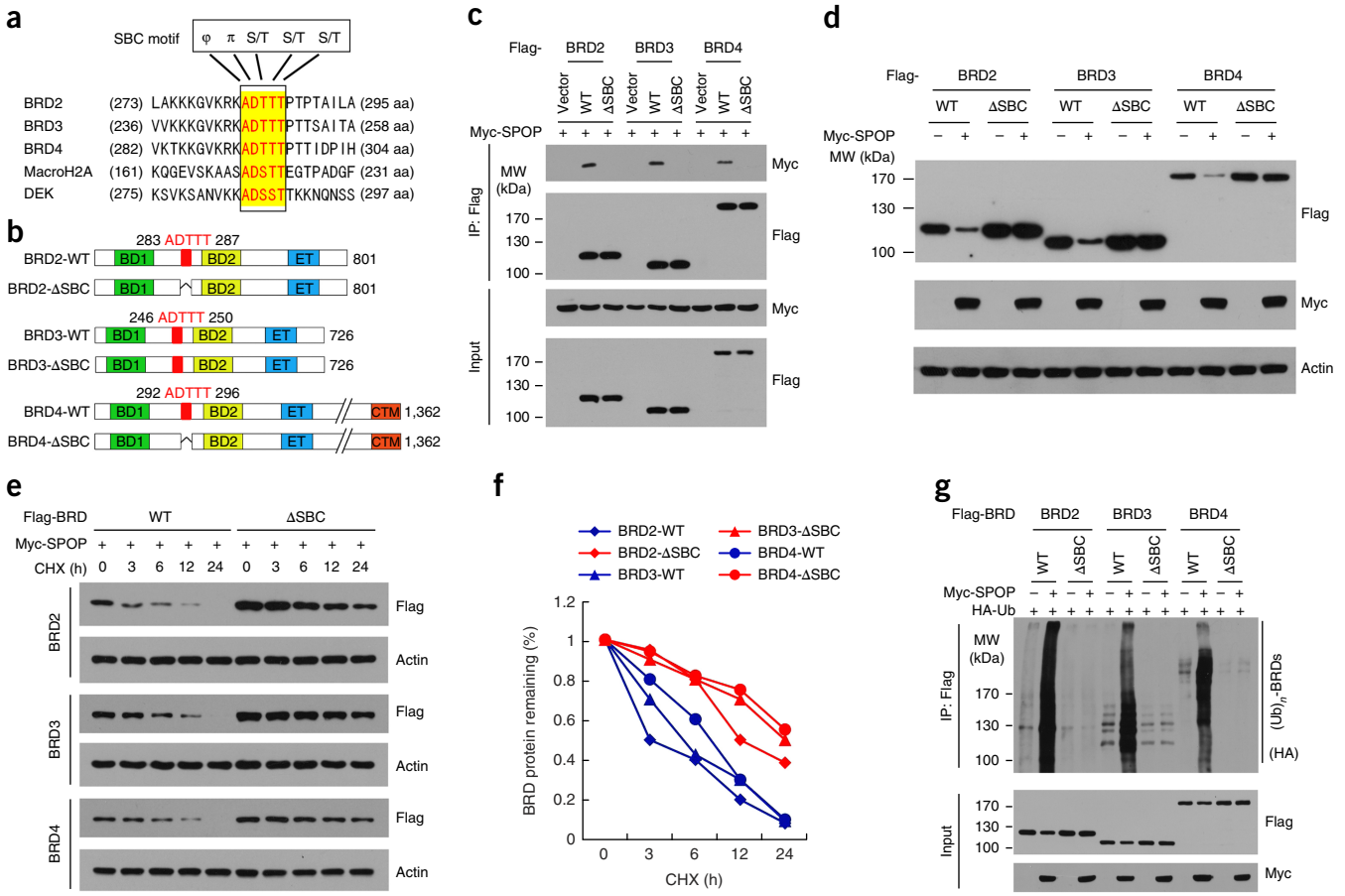

Figure 2 The SBC motif in BET proteins is a SPOP-recognized degron. (**a**) Amino acid sequence alignment of putative SBC motifs in BRD2, BRD3 and BRD4. MacroH2A and DEK are known SPOP substrates containing well-characterized SBC motifs. Homologous amino acids among the indicated proteins are depicted in red. (**b**) Diagram showing wild-type BET proteins and SBC-motif-deleted mutants (ΔSBC). The SBC is depicted in red. (**c**) Western blots of WCL and samples from co-IP with anti-Flag antibody in 293T cells transfected with the indicated constructs and treated with 20 μM MG-132 for 8 h. (**d**) Western blots of WCL from 293T cells transfected with the indicated constructs. (**e**) Western blots of WCL from 293T cells transfected with the indicated constructs, treated with 50 μg/ml cycloheximide (CHX) and harvested at different time points. (**f**) Quantification of the western blots carried out in **e**. At each time point, the intensity of BET protein was normalized to the intensity of actin and then to the value at 0 h. (**g**) Western blots of the products of *in vivo* ubiquitination assays from 293T cells transfected with the indicated constructs and treated with 20 μM MG-132 for 8 h.

in different cohorts of prostate cancer[10,11]. Immunohistochemistry (IHC) analysis showed that approximately 85%, 92% and 85% of *SPOP*-mutated tumors exhibited strong or intermediate staining for BRD2, BRD3 and BRD4, respectively (**Fig. 3d**,**e**). In contrast, ≤40% of tumors with wild-type *SPOP* exhibited strong or intermediate staining for the BET proteins, whereas the majority of them (approximately 71%, 66% and 59% for BRD2, BRD3 and BRD4, respectively) exhibited weak staining (**Fig. 3d**,**e**). Expression of the corresponding mRNAs was lower in *SPOP*-mutated tumors than in specimens with wild-type *SPOP* in our cohorts, although the differences between the groups did not reach statistical significance (except in the case of *BRD2*) (**Supplementary Fig. 2c**). A similar trend was observed in The Cancer Genome Atlas (TCGA) data set (**Supplementary Fig. 2d**). These findings indicate that BET protein levels are elevated in *SPOP*-mutated prostate cancer specimens, and this is unlikely to be caused by increases in corresponding mRNA levels.

Small-molecule inhibitors of BET proteins are actively being tested as promising epigenetically targeted therapeutics for cancer[1,3–9,17,18]. We examined whether SPOP-mediated degradation of BET proteins influences the anticancer efficacy of BET inhibitors in prostate cancer cells. Knockdown of endogenous SPOP by short hairpin RNAs (shRNAs) not only increased BET protein levels but also enhanced proliferation of C4-2 prostate cancer cells—this effect was abolished by combined knockdown of BRD2, BRD3 and BRD4 (**Supplementary Fig. 3a**–**g**). In accordance with a previous report[6], we demonstrated that the BET inhibitor JQ1 robustly inhibited growth of C4-2 prostate cancer cells, but this effect was greatly attenuated in SPOP-knockdown cells (**Supplementary Fig. 3a**–**c**). SPOP-depletion-mediated resistance to JQ1 was reversed by knockdown of BRD4 alone (**Supplementary Fig. 3h**–**j**). However, BRD4-knockout cells became highly resistant to JQ1 when BRD2 and BRD3 were mostly depleted (**Supplementary Fig. 3k**,**l**). This result is not surprising, as little or no druggable target (BET proteins) was present in these cells. These data suggest that BET protein levels may represent a molecular determinant for JQ1 sensitivity in SPOP-deficient prostate cancer cells.

F133 is the most frequently mutated residue in SPOP[10]. To recapitulate this scenario, we introduced the F133V mutant of SPOP into C4-2 and 22Rv1 cells, which harbor wild-type *SPOP*. Expression of SPOP-F133V not only induced accumulation of BET proteins but also caused a significant increase in cellular proliferation in both cell lines in comparison to cells expressing empty vector (**Supplementary Fig. 3m**,**n**). Whereas JQ1 treatment inhibited growth of C4-2 and

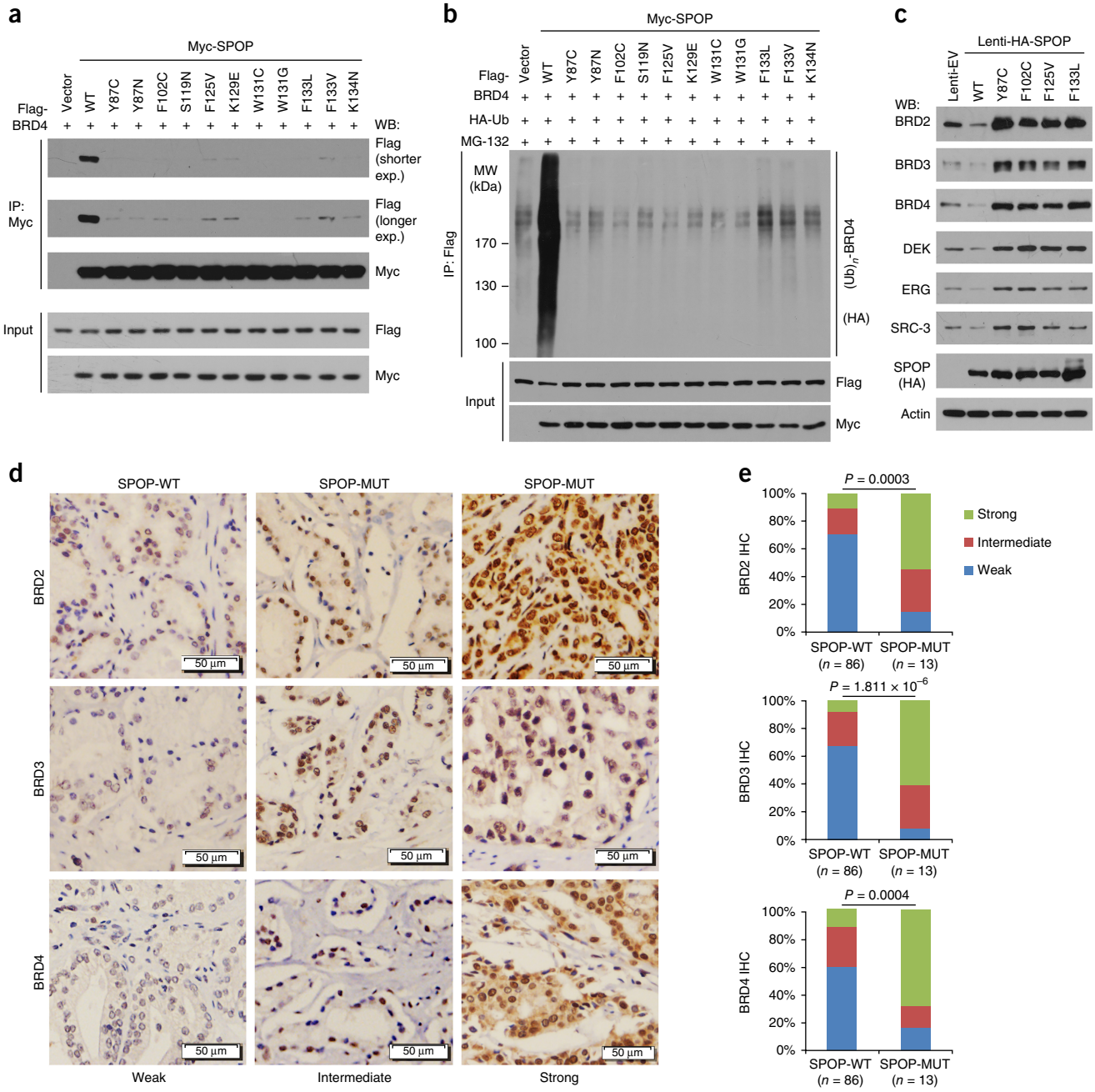

Figure 3 Expression of BET proteins is elevated in SPOP-mutant-expressing prostate cancer cell lines and specimens from patients with prostate cancer. (**a**) Western blots of WCL and samples from co-IP with anti-Flag antibody in 293T cells transfected with the indicated Myc- or Flag-tagged constructs and treated with 20 μM MG-132 for 8 h. Exp., exposure. (**b**) Western blots of the products of *in vivo* ubiquitination assays from 293T cells transfected with the indicated Myc- or Flag-tagged constructs and treated with 20 μM MG-132 for 8 h. (**c**) Western blots of the indicated proteins in WCL from C4-2 cells infected with empty vector (EV) or lentivirus expressing wild-type or mutant SPOP. (**d**) Representative images of BRD2, BRD3 and BRD4 IHC from 99 cases of prostate cancer expressing wild-type SPOP or mutant SPOP (MUT). (**e**) Quantitative data for the BET protein staining in **d**. Statistical significance was determined by Wilcoxon rank-sum test.

22Rv1 cells infected with empty vector, this effect was largely impeded in SPOP-F133V-expressing cells (**Supplementary Fig. 3n**). SPOP-F133V expression also caused similar resistance to another BET inhibitor, I-BET, in C4-2 and 22Rv1 cells (**Supplementary Fig. 3o–q**). We further found that the SPOP-F133V mutant conferred JQ1 resistance in tumor xenografts of C4-2 cells in mice (**Fig. 4a–c**). SPOP-F133V-mediated resistance to JQ1 was completely reversed by combined depletion of BRD2, BRD3 and BRD4 in C4-2 cells *in vitro* and in C4-2 xenografts in mice (**Fig. 4a–c** and **Supplementary Fig. 4a–c**). SPOP-F133V expression also induced accumulation of the known SPOP substrates ERG, DEK and SRC-3 (refs. 12–14) in C4-2 and 22Rv1 cells and in C4-2-derived tumors in mice (**Supplementary Figs. 3m** and **4d**). However, JQ1 treatment largely decreased ERG expression (**Supplementary Figs. 3m** and **4d**,**e**), which is in keeping with similar findings in acute myeloid leukemia cells[19]. Knockdown of ERG by shRNA had no overt effect on SPOP-F133V-mediated resistance

to JQ1 in C4-2 cells, and similar results were obtained in DEK-knockdown cells (**Supplementary Fig. 4e**,**f**). SRC-3 knockdown slightly sensitized SPOP-F133V-expressing cells to JQ1, but the effect was not statistically significant (**Supplementary Fig. 4e**,**f**). Thus, our data suggest that *SPOP*-mutation-conferred resistance to BET inhibitors is largely mediated by increased BRD2, BRD3 and BRD4 protein levels in prostate cancer cells.

Next, we investigated the role of *SPOP*-mutation-induced accumulation of BET proteins in resistance to BET inhibitors in clinically oriented models. Among the three examined organoid lines derived from individuals with prostate cancer, one harbored a p.W131R substitution in SPOP. W131 constitutes a conserved residue in the substrate-binding cleft[10]. We demonstrated that the SPOP-W131R mutant was deficient in binding to and mediating ubiquitination and degradation of BRD4 (**Supplementary Fig. 5a–c**). Most notably, the organoid encoding SPOP-W131R expressed more BET proteins and was resistant to JQ1 in comparison to its two counterparts encoding wild-type SPOP under both 2D and 3D growth conditions (**Supplementary Fig. 5d–g**). These data indicate that *SPOP* mutation confers resistance to BET inhibitors in primary cultures derived from individuals with prostate cancer.

It is worth noting that BET inhibitors have been shown to induce BRD4 accumulation in different cell types, but the underlying mechanism is unclear[6,20]. We demonstrated that the effect of the JQ1 inhibitor occurred at the post-transcriptional level (**Fig. 4a** and **Supplementary Figs. 3m** and **6a**,**b**). We further showed that JQ1 diminished SPOP interaction with BRD2, BRD3 and BRD4, partially blocked SPOP-induced ubiquitination and degradation of these proteins, and prolonged BET protein half-lives, even in SPOP-F133V-expressing cells (**Supplementary Fig. 6c–h**). Thus, while inhibiting BET protein activities, BET inhibitors undesirably disturb their proteolysis; this effect appears to be mediated by SPOP-dependent and SPOP-independent mechanisms.

To define the signaling pathways that mediate resistance to BET inhibitors in *SPOP*-mutated cells, we performed transcriptome analysis in control (empty vector) and SPOP-F133V-expressing C4-2 cells treated with JQ1 or left untreated. Through unsupervised cluster analysis of differentially expressed genes, we identified 5,079 genes that were downregulated by JQ1 in both control and SPOP-F133V-expressing cells, including *MYC* and *AR*, encoding two known proteins in signaling pathways affected by BET inhibitors[3,5,6] (**Supplementary Fig. 7a**). A previous study suggested that MYC may not be the major anticancer target of JQ1 in prostate cancer cells[6]. In agreement with this report, we found that JQ1 treatment markedly decreased MYC protein levels, in accordance with substantial reduction of BRD4 binding in the *MYC* gene enhancer in both JQ1-sensitive (control) and JQ1-resistant (SPOP-F133V-expressing) C4-2 cells (**Supplementary Fig. 7b–d**). JQ1 also strongly decreased AR protein levels, BRD4 binding in the *AR* gene promoter and AR transcriptional activity in both control and SPOP-F133V-expressing cells (**Supplementary Fig. 7b–f**), and further knockdown of AR by shRNA did not affect sensitivity to JQ1 in these cells (**Supplementary Fig. 7g**,**h**). Collectively, these findings suggest that resistance to BET inhibitors in *SPOP*-mutated prostate cancer cells is likely mediated by MYC- and AR-independent pathways.

Further analysis of the RNA-seq data identified 1,017 genes whose expression was suppressed by JQ1 in control cells but remained unchanged or was upregulated in SPOP-F133V-expresing cells (**Fig. 4d**). Of these genes, 129 were highly upregulated in *SPOP*-mutated prostate tumors as compared to those expressing wild-type *SPOP* in the TCGA cohort (**Fig. 4e** and **Supplementary Table 4**). Notably, these aberrantly upregulated genes significantly overlapped with the BRD4 target genes identified in C4-2 cells transfected to express SPOP-F133V as well as in C4-2 cells expressing hemagglutinin (HA)-tagged BRD4 (**Fig. 4f** and **Supplementary Fig. 8a–c**). In Ingenuity pathway analysis of the overlapping genes, the top pathway was the cholesterol biosynthesis pathway, and four members of this pathway—*FDFT1*, *DHCR24*, *DHCR7* and *MVD*—were upregulated in *SPOP*-mutated tumors (**Fig. 4e**,**f**). Cholesterol-rich lipid rafts have been linked to AKT activation and prostate cancer cell survival[21–23]. As the Rho GTPase family member RAC1 can also activate the AKT–mTORC1 pathway by directly binding to mTOR[24,25], and *RAC1* mRNA expression was upregulated in *SPOP*-mutated tumors (**Fig. 4e**), we chose to focus on these two pathways. Meta-analysis of published BRD4 ChIP–seq data also showed BRD4 binding at the *RAC1* locus in different cell types (**Supplementary Fig. 8d**). RNA-seq analysis showed that the genes whose transcription was altered by BET protein overexpression in C4-2 cells significantly overlapped with the genes associated with JQ1 resistance, including *RAC1*, in cells expressing the SPOP-F133V mutant (**Supplementary Fig. 8e–g** and **Supplementary Table 5**). ChIP–seq and ChIP–qPCR assays showed that BRD4 readily bound at the *RAC1* gene promoter in control cells, but binding was greatly enhanced by expression of SPOP-F133V or HA-BRD4 (**Fig. 4f**,**g** and **Supplementary Fig. 8c**,**h**). Increased BRD4 binding is unlikely to be caused by histone acetylation changes, as expression of SPOP-F133V or the BRD proteins had no effect on the levels of H3K27ac, H4K5ac and H4K8ac both globally and at the *RAC1* locus (**Supplementary Fig. 8i**,**j**). BRD4-dependent regulation of *RAC1* was confirmed by gene-knockdown experiments (**Supplementary Fig. 8k**,**l**), providing further evidence that *RAC1* is a bona fide BRD4 target gene. Additionally, increased BRD4 binding, *RAC1* mRNA levels and RAC1 protein expression correlated with high levels of BRD4 protein in JQ1-resistant cells expressing SPOP-F133V in comparison to untreated control cells (**Fig. 4g** and **Supplementary Fig. 8c**,**m**,**n**). Furthermore, SPOP-F133V expression substantially increased phosphorylation of AKT and S6K, a kinase downstream of mTORC1, in both C4-2 and 22Rv1 cells regardless of JQ1 treatment (**Supplementary Figs. 3m** and **8o**). Knockdown of RAC1 not only inhibited SPOP-F133V-augmented AKT and S6K phosphorylation, but also abolished SPOP-F133V-mediated resistance to JQ1 in C4-2 cells (**Supplementary Fig. 8o**,**p**).

ChIP–seq and ChIP–qPCR assays showed that BRD4 readily bound in the promoters of the cholesterol-synthesis-associated genes *FDFT1*, *DHCR24*, *DHCR7* and *MVD* in control cells. This binding was enhanced by SPOP-F133V expression (**Supplementary Fig. 9a–c**); the effect is unlikely to be caused by global or locus-specific histone acetylation changes (**Supplementary Figs. 8i** and **9d**). Knockdown of BRD4 greatly decreased expression of these genes at the mRNA and protein levels in both control and SPOP-F133V-expressing cells (**Supplementary Figs. 8n** and **9e**). With concomitant induction of BRD4 protein levels, SPOP-F133V upregulated the expression of cholesterol-synthesis-associated genes at both the mRNA and protein levels and enhanced BRD4 binding in their promoters (**Supplementary Fig. 9b**,**c**,**e**,**f**). JQ1 treatment strongly inhibited expression of these genes and BRD4 binding at their promoters in control cells, but the effect was not pronounced in SPOP-F133V-expressing cells (**Supplementary Fig. 9b**,**c**,**f**,**g**). Combined depletion of these cholesterol-synthesis-related genes abolished SPOP-F133V-induced activation of the AKT–mTORC1 pathway and JQ1 resistance in C4-2 cells (**Supplementary Fig. 9h**,**i**). As with overexpression

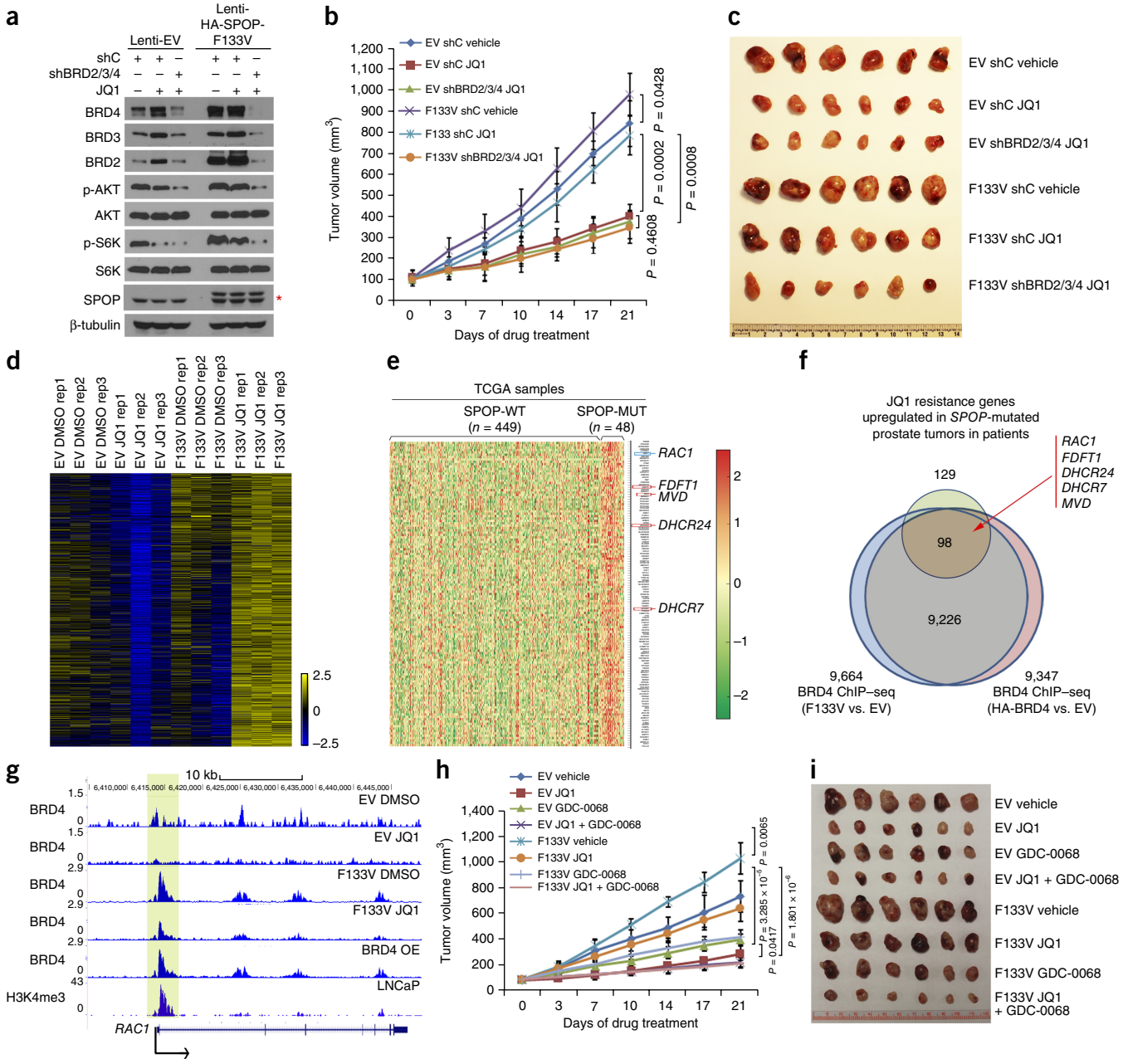

Figure 4 Mechanism of BET inhibitor resistance in prostate cancer cells expressing SPOP mutants. (**a**) Western blots of the indicated proteins, including phosphorylated AKT (p-AKT; S473) and phosphorylated S6K (p-S6K; T389), in C4-2 cells infected with empty vector or lentivirus expressing SPOP-F133V in combination with control shRNA or BRD2-, BRD3- and BRD4-specific shRNAs (shBRD2/3/4). Cells were treated with JQ1 (1 μM) or left untreated for 24 h before they were harvested. The red asterisk indicates the exogenous SPOP-F133V mutant. (**b**) Volume of C4-2 xenograft tumors in mice (n = 6/group) following treatment with the indicated drugs. Data are shown as means ± s.d. Statistical significance was determined by two-tailed Student's t-test for tumors at day 21 of drug treatment. (**c**) Image of tumors isolated from each group of mice in **b** at day 21 of drug treatment. (**d**) Heat map of RNA-seq data showing a cluster of genes (n = 1,017) that were differentially expressed in C4-2 cells infected with empty vector or lentivirus expressing SPOP-F133V and treated with vehicle (DMSO) or JQ1 (1 μM) for 24 h. Data from three replicates are included for each condition. (**e**) Heat map showing 129 JQ1-resistance-associated genes, the expression of which was upregulated in *SPOP*-mutated prostate tumors as compared to tumors with wild-type *SPOP* in the TCGA cohort. The color keys represent the median-centered $\log_2$ value of fragments per kilobase of transcript per million mapped reads, ranging from –2.5 to 2.5 in **d** and from –2 to 2 in **e**. (**f**) Venn diagram showing that JQ1-resistance-associated genes upregulated in *SPOP*-mutated prostate tumors significantly overlap with genes bound by BRD4 in response to both SPOP-F133V and HA-BRD4 overexpression in C4-2 cells ($P = 9.407 \times 10^{-12}$, permutation test). (**g**) UCSC Genome Browser screenshots showing BRD4 ChIP–seq signal profiles in the *RAC1* gene locus in C4-2 cells infected with empty vector or expressing SPOP-F133V or HA-BRD4 and treated with DMSO or JQ1 (1 μM) for 24 h. H3K4me3 ChIP–seq data were acquired from LNCaP cells as reported previously[33]. OE, overexpression. (**h**) Volume of C4-2 xenograft tumors in mice (n = 6/group) following treatment with the indicated drugs. Data are shown as means ± s.d. Statistical significance was determined by a two-tailed Student's t-test for tumors at day 21 of drug treatment. (**i**) Image of tumors isolated from each group of mice in **h** at day 21 of drug treatment.

of the SPOP mutants, moderate overexpression of the BET proteins increased cholesterol biosynthesis and AKT–mTORC1 activation (**Supplementary Figs. 8e** and **9j**). These data imply that both the RAC1 and cholesterol synthesis pathways are required to mediate *SPOP*-mutation-induced AKT–mTORC1 activation and JQ1 resistance (**Supplementary Fig. 9k**).

We further demonstrated that AP-1 (a dimer of c-JUN and c-FOS) bound to both *RAC1* and the promoters of cholesterol-synthesis-associated genes (**Supplementary Fig. 9l**,**m**). Although expression of c-JUN and c-FOS was not affected by *SPOP* mutation, knockdown of both abolished SPOP-F133V-induced upregulation of *RAC1* and cholesterol-synthesis-associated genes and activation of AKT–mTORC1 without disturbing BRD4 expression (**Supplementary Fig. 9n**–**p**). It has recently been shown that the AKT–mTORC1 pathway is activated in the prostates of SPOP-F133V knock-in mice, and this effect is partially mediated by increased SRC-3 expression[26]. We also demonstrated that SRC-3 knockdown only partially decreased SPOP-F133V-induced AKT–mTORC1 activation by selectively affecting expression of *RAC1* and the cholesterol-synthesis-associated genes and it slightly, but not significantly, diminished SPOP-F133V-mediated JQ1 resistance (**Supplementary Figs. 4f** and **9p**), reinforcing the notion that SPOP-F133V-mediated AKT–mTORC1 activation is partially mediated by SRC-3. In contrast, depletion of BET proteins almost completely abolished SPOP-F133V-induced AKT–mTORC1 activation, upregulation of *RAC1* and the cholesterol-synthesis-associated genes, and BET inhibitor resistance (**Fig. 4a**–**c** and **Supplementary Fig. 9p**).

It has been shown that treatment with a PI3K inhibitor induces expression of receptor tyrosine kinases (RTKs), including receptor tyrosine protein kinase ERBB-3 (HER3), insulin-like growth factor 1 receptor (IGF1R) and insulin receptor (INSR), and this induction is mediated by BRD4 but blocked by BET inhibitor[27]. However, BET inhibitor treatment alone has no effect on RTK expression[27]. Similarly, no effect of JQ1 on expression of these proteins was detected in either JQ1-sensitive (control) or JQ1-resistant (SPOP-F133V-expressing) C4-2 cells (**Supplementary Fig. 10a**). We further demonstrated that neither mTORC1 activity (S6K phosphorylation) nor JQ1-resistant growth was affected by knockdown of HER3, IGF1R or INSR individually in SPOP-F133V-expressing C4-2 cells (**Supplementary Fig. 10b**–**d**). These data rule out a potential role for these RTKs in SPOP-F133V-induced AKT activation and JQ1 resistance in these cells. In contrast, individual knockdown of AKT (AKT1, AKT2 and AKT3), mTOR or Raptor abolished JQ1-resistant growth of SPOP-F133V-expressing C4-2 cells (**Supplementary Fig. 10e**–**g**). Similar results were obtained by treating SPOP-F133V-expressing cells with the allosteric AKT inhibitor MK2206 (**Supplementary Fig. 10h**). Most recently, a first-in-human phase 1 study has shown that ipatasertib (GDC-0068), a new ATP-competitive AKT inhibitor, exhibits effective antitumor activity in patients with solid tumors[28]. We demonstrated that GDC-0068 treatment of SPOP-mutant-expressing cells not only abolished *SPOP*-mutation-induced activation of AKT downstream pathways but also completely overcame *SPOP*-mutation-conferred resistance to BET inhibitors in C4-2 cells in culture and C4-2-derived tumors in mice (**Fig. 4h**,**i** and **Supplementary Fig. 10i**). These findings highlight the major role of AKT inhibition in overcoming BET inhibitor resistance in *SPOP*-mutated prostate cancer (**Supplementary Fig. 10j**).

In summary, our findings demonstrate that BRD2, BRD3 and BRD4 are degradation substrates of SPOP. We uncover that *SPOP* mutation not only induces accumulation of these proteins but also confers intrinsic resistance to BET inhibitors in prostate cancer cells, suggesting that, besides *SPOP* mutations, elevation of BET proteins can be a biomarker for prediction of BET inhibitor resistance in patients with prostate cancer. In TCGA data, *SPOP*-mutated tumors have the highest AR transcriptional activity among all the genotypically distinct subsets of prostate cancer[11]. This observation is further supported by other reports that the protein levels of AR and its co-regulators, such as SRC-3, ERG and TRIM24, are stabilized by SPOP mutants in prostate cancer[13,14,29,30]. These findings stress that aberrant activation of AR not only represents a key event contributing to the pathophysiology resulting from *SPOP* mutations in prostate cancer, but also can be targeted for treatment of *SPOP*-mutated tumors. In accordance with recent reports that JQ1 blocks growth of SPOP-proficient prostate cancer cells by inhibiting AR expression and activity[6,31], we demonstrate that expression of AR and the examined genes downstream of it was inhibited by JQ1 in cells expressing wild-type SPOP and SPOP-F133V. Similarly, BET inhibitor treatment also decreases expression of ERG and its downstream targets[19,32], in keeping with our finding that knockdown of ERG has little or no effect on *SPOP*-mutation-induced resistance to BET inhibitors. These data suggest that intrinsic BET inhibitor resistance develops independently of the elevated AR and ERG signaling in *SPOP*-mutated prostate cancer cells. It is worth noting that both AR and ERG directly interact with the bromodomain of BRD4, and these interactions are both sensitive to JQ1 (refs. 6,19,32). At present, it is unclear why AR and ERG are vulnerable to BET inhibition irrespective of elevated BET protein levels in *SPOP*-mutated cells, and whether this vulnerability is due to their JQ1-sensitive binding of BET proteins (**Supplementary Fig. 10j**) warrants further investigation. We also show that expression of SPOP-F133V not only increases the basal levels of phosphorylation of proteins in the AKT–mTORC1 pathway, but also largely impedes JQ1-induced inhibition of their phosphorylation. Accordingly, we uncover that the expression levels of *RAC1* and cholesterol-biosynthesis-associated genes, both of which are required for activation of the AKT–mTORC1 pathway[21,23–25], are upregulated in individuals with *SPOP*-mutated prostate tumors. Therefore, in addition to demonstrating the essential role of elevated BET protein levels and activation of the AKT–mTORC1 pathway in resistance to BET inhibition as a consequence of *SPOP* mutation in prostate cancer cells (**Supplementary Fig. 10j**), we also provide evidence that targeting the AKT pathway using new therapeutic agents, such as the novel AKT inhibitor ipatasertib, could be a viable treatment option to overcome BET inhibitor resistance in *SPOP*-mutated prostate cancer.

URLs. Burrows–Wheeler aligner, http://bio-bwa.sourceforge.net/; GREAT, http://bejerano.stanford.edu/great/public/html/.

METHODS

Methods, including statements of data availability and any associated accession codes and references, are available in the online version of the paper.

Note: Any Supplementary Information and Source Data files are available in the online version of the paper.

ACKNOWLEDGMENTS

This work was supported in part by grants from the National Institutes of Health (CA134514, CA130908 and CA193239 to H.H.), the US Department of Defense (W81XWH-09-1-622 to H.H.), the National Natural Science Foundation of China (81672558 and 81201533 to C.W.; 81572768 to P.Z.; 31560320 to D. Wang; 31400753 to K.G.), and the National Key Research and Development Plan of China–Precision Medicine Project (2016YFC0902202 to Y.S., C.W. and S.R.).

AUTHOR CONTRIBUTIONS

H.H. and C.W. conceived the study. P.Z., D.W., Y. Zhao, S.R., K.G., Z.Y., S.W., C.-W.P., Y. Zhu, Y.Y., D. Wu, Y.H., D. Lu, L.Y., S.Z., Y.L., D. Lin, Y.W. and Y.C. acquired patient samples, generated organoids, and performed the experiments and data analyses. Z.Y. and L.W. performed bioinformatics analyses. X.L. and J.Z. supervised histological and IHC data analyses. H.H., C.W. and Y.S. wrote the paper.

COMPETING FINANCIAL INTERESTS

The authors declare no competing financial interests.

1. Filippakopoulos, P. *et al.* Selective inhibition of BET bromodomains. *Nature* **468**, 1067–1073 (2010).
2. Nicodeme, E. *et al.* Suppression of inflammation by a synthetic histone mimic. *Nature* **468**, 1119–1123 (2010).
3. Delmore, J.E. *et al.* BET bromodomain inhibition as a therapeutic strategy to target c-Myc. *Cell* **146**, 904–917 (2011).
4. Dawson, M.A. *et al.* Inhibition of BET recruitment to chromatin as an effective treatment for *MLL*-fusion leukaemia. *Nature* **478**, 529–533 (2011).
5. Zuber, J. *et al.* RNAi screen identifies Brd4 as a therapeutic target in acute myeloid leukaemia. *Nature* **478**, 524–528 (2011).
6. Asangani, I.A. *et al.* Therapeutic targeting of BET bromodomain proteins in castration-resistant prostate cancer. *Nature* **510**, 278–282 (2014).
7. Fong, C.Y. *et al.* BET inhibitor resistance emerges from leukaemia stem cells. *Nature* **525**, 538–542 (2015).
8. Rathert, P. *et al.* Transcriptional plasticity promotes primary and acquired resistance to BET inhibition. *Nature* **525**, 543–547 (2015).
9. Shu, S. *et al.* Response and resistance to BET bromodomain inhibitors in triple-negative breast cancer. *Nature* **529**, 413–417 (2016).
10. Barbieri, C.E. *et al.* Exome sequencing identifies recurrent *SPOP*, *FOXA1* and *MED12* mutations in prostate cancer. *Nat. Genet.* **44**, 685–689 (2012).
11. Cancer Genome Atlas Research Network. The molecular taxonomy of primary prostate cancer. *Cell* **163**, 1011–1025 (2015).
12. Theurillat, J.P. *et al.* Ubiquitylome analysis identifies dysregulation of effector substrates in SPOP-mutant prostate cancer. *Science* **346**, 85–89 (2014).
13. Geng, C. *et al.* Prostate cancer–associated mutations in speckle-type POZ protein (SPOP) regulate steroid receptor coactivator 3 protein turnover. *Proc. Natl. Acad. Sci. USA* **110**, 6997–7002 (2013).
14. An, J. *et al.* Truncated ERG oncoproteins from TMPRSS2-ERG fusions are resistant to SPOP-mediated proteasome degradation. *Mol. Cell* **59**, 904–916 (2015).
15. Zhuang, M. *et al.* Structures of SPOP–substrate complexes: insights into molecular architectures of BTB–Cul3 ubiquitin ligases. *Mol. Cell* **36**, 39–50 (2009).
16. Blattner, M. *et al. SPOP* mutations in prostate cancer across demographically diverse patient cohorts. *Neoplasia* **16**, 14–20 (2014).
17. Mertz, J.A. *et al.* Targeting MYC dependence in cancer by inhibiting BET bromodomains. *Proc. Natl. Acad. Sci. USA* **108**, 16669–16674 (2011).
18. Lovén, J. *et al.* Selective inhibition of tumor oncogenes by disruption of super-enhancers. *Cell* **153**, 320–334 (2013).
19. Roe, J.S., Mercan, F., Rivera, K., Pappin, D.J. & Vakoc, C.R. BET bromodomain inhibition suppresses the function of hematopoietic transcription factors in acute myeloid leukemia. *Mol. Cell* **58**, 1028–1039 (2015).
20. Lu, J. *et al.* Hijacking the E3 ubiquitin ligase cereblon to efficiently target BRD4. *Chem. Biol.* **22**, 755–763 (2015).
21. Zhuang, L., Lin, J., Lu, M.L., Solomon, K.R. & Freeman, M.R. Cholesterol-rich lipid rafts mediate AKT-regulated survival in prostate cancer cells. *Cancer Res.* **62**, 2227–2231 (2002).
22. Yue, S. *et al.* Cholesteryl ester accumulation induced by PTEN loss and PI3K/AKT activation underlies human prostate cancer aggressiveness. *Cell Metab.* **19**, 393–406 (2014).
23. Lasserre, R. *et al.* Raft nanodomains contribute to Akt/PKB plasma membrane recruitment and activation. *Nat. Chem. Biol.* **4**, 538–547 (2008).
24. Saci, A., Cantley, L.C. & Carpenter, C.L. Rac1 regulates the activity of mTORC1 and mTORC2 and controls cellular size. *Mol. Cell* **42**, 50–61 (2011).
25. Esen, E. *et al.* WNT–LRP5 signaling induces Warburg effect through mTORC2 activation during osteoblast differentiation. *Cell Metab.* **17**, 745–755 (2013).
26. Blattner, M. *et al. SPOP* mutation drives prostate tumorigenesis *in vivo* through coordinate regulation of PI3K/mTOR and AR signaling. *Cancer Cell* **31**, 436–451 (2017).
27. Stratikopoulos, E.E. *et al.* Kinase and BET inhibitors together clamp inhibition of PI3K signaling and overcome resistance to therapy. *Cancer Cell* **27**, 837–851 (2015).
28. Saura, C. *et al.* A first-in-human phase I study of the ATP-competitive AKT inhibitor ipatasertib demonstrates robust and safe targeting of AKT in patients with solid tumors. *Cancer Discov.* **7**, 102–113 (2017).
29. An, J., Wang, C., Deng, Y., Yu, L. & Huang, H. Destruction of full-length androgen receptor by wild-type SPOP, but not prostate-cancer-associated mutants. *Cell Rep.* **6**, 657–669 (2014).
30. Groner, A.C. *et al.* TRIM24 is an oncogenic transcriptional activator in prostate cancer. *Cancer Cell* **29**, 846–858 (2016).
31. Chan, S.C. *et al.* Targeting chromatin binding regulation of constitutively active AR variants to overcome prostate cancer resistance to endocrine-based therapies. *Nucleic Acids Res.* **43**, 5880–5897 (2015).
32. Blee, A.M., Liu, S., Wang, L. & Huang, H. BET bromodomain-mediated interaction between ERG and BRD4 promotes prostate cancer cell invasion. *Oncotarget* **7**, 38319–38332 (2016).
33. Wang, D. *et al.* Reprogramming transcription by distinct classes of enhancers functionally defined by eRNA. *Nature* **474**, 390–394 (2011).

ONLINE METHODS

Antibodies and chemicals. The following antibodies were used: SPOP (ab137537, Abcam), SPOP (16750-1-AP, Proteintech), BRD2 (A302-583A, Bethyl), BRD2 (ab139690, Abcam), BRD3 (A302-368A, Bethyl), BRD4 (ab128874, Abcam), BRD4 (A301-985A, Bethyl), MYC (9E10, Sigma-Aldrich), MYC (sc-40, Santa Cruz Biotechnology), Flag (M2, Sigma), HA (MM5-101R, Convance), actin (AC-74, Sigma-Aldrich), DEK (13962S, Cell Signaling Technology), ERG (sc-352, Santa Cruz Biotechnology), AR (sc-816, Santa Cruz Biotechnology), SRC-3 (611104, BD), phospho-AKT-S473 (9471, Cell Signaling Technology), phospho-AKT-T308 (9275, Cell Signaling Technology), AKT (9272, Cell Signaling Technology), phospho-S6K-T389 (9205, Cell Signaling Technology), S6K (9202, Cell Signaling Technology), β-tubulin (T4026, Sigma-Aldrich), RAC1 (23A8, BD), FDFT1 (ab195046, Abcam), DHCR24 (ab137845, Abcam), DHCR7 (ab103296, Abcam), MVD (ab12906, Abcam), HER3 (12708S, Cell Signaling Technology), INSR (ab131238, Abcam), IGF-1R (sc-9038, Santa Cruz Biotechnology), mTOR (2972, Cell Signaling Technology) and Raptor (24C12, Cell Signaling Technology). MG-132 and cycloheximide were purchased from Sigma-Aldrich; MLN4924, bortezomib and MK2206 were purchased from Selleckchem. JQ1 was kindly provided by J. Bradner (Harvard Medical School) and purchased from Sigma-Aldrich. I-BET762 (I-BET) was purchased from MedchemExpress. GDC-0068 was purchased from Calbiochem.

Plasmids and mutagenesis. Expression vectors for wild-type SPOP and mutants were described previously[29]. Flag-BRD2 and Flag-BRD3 constructs were obtained from S.J. Flint (Princeton University). Flag-BRD4 constructs were obtained from T. Honjo (Kyoto University). Flag-BRD2, Flag-BRD3 and Flag-BRD4 mutants were generated with the KOD Plus Mutagenesis Kit (Toyobo) following the manufacturer's instructions. lenticrisprV2 plasmid (52961) was purchased from Addgene.

Cell culture, transfection and lentivirus infection. LNCaP, 22Rv1 and 293T cells were obtained from the American Type Culture Collection (ATCC). C4-2 cells were purchased from Uro Corporation. BPH-1 cells were kindly provided by S. Hayward (Northshore University Health System, Chicago)[34]. 293T cells were maintained in DMEM supplemented with 10% FBS, and LNCaP, C4-2, 22Rv1 and BPH-1 cells were maintained in RPMI medium supplemented with 10% FBS. Cells were transiently transfected using Lipofectamine RNAi MAX (for siRNA transfection) or Lipofectamine 3000 (for plasmid transfection) (Thermo Fisher Scientific) according to the manufacturer's instructions. pTsin-HA-SPOP-F133V mutant expression or pLKO-based gene-knockdown lentiviral vectors or lenticrisprV2-BRD4and packing constructs were transfected into 293T cells. Virus-containing supernatant was collected 48 h after transfection. C4-2 and 22Rv1 cells were infected with virus-containing supernatant in the presence of polybrene (8 μg/ml) and were then selected in growth medium containing 1.5 μg/ml puromycin. Sequences of gene-specific shRNAs are listed in **Supplementary Table 6**. All the cell lines used have been tested and authenticated by karyotyping, and prostate cancer cell lines have also been authenticated by examining AR expression and *SPOP* mutation status. Plasmocin (Invivogen) was added to cell culture media to prevent mycoplasma contamination. Mycoplasma contamination was tested for regularly using the Lookout Mycoplasma PCR Detection Kit from Sigma-Aldrich.

Organoid cultures and cell viability assays. Organoid cells were kindly provided by Y. Chen (MSKCC) and cultured according to the methodology described previously[35]. In brief, organoid cells were embedded in 40 μl of Matrigel for each drop and cultured in FBS-free DMEM/F-12 medium supplemented with several growth factors including epidermal growth factor (EGF), fibroblast growth factor 2 (FGF2) and FGF10. Cell viability assays were conducted by plating 2,000 organoid cells per well of a collagen-coated 96-well cell culture plate in 100 ml of medium with vehicle (DMSO) control or JQ1 (0.05–1 μM). Viable cells were counted by using a CellTiter-Glo (Promega) Luminescent Cell Viability Assay Kit.

Samples from individuals with prostate cancer. Treatment-naive prostate cancer and matched benign tissues were collected from the radical prostatectomy series at Shanghai Changhai Hospital, and the institutional review board of the hospital approved the experimental protocols; informed consent was obtained from each patient. H&E slides of frozen and formalin-fixed, paraffin-embedded (FFPE) human tumor tissues and matched benign tissues were examined by a general pathologist and a genitourinary pathologist to confirm histological diagnoses and Gleason score and to verify the high-density cancer foci (>80%) of the selected tumor tissue. The frozen blocks for DNA and RNA extraction, followed by ten consecutive 10-μm sections of each tumor, were examined by the pathologists as described above. These qualified samples were then used for DNA and RNA isolation. FFPE tissues were used for IHC analyses.

Detection of prostate cancer specimens with *SPOP* mutations by whole-genome and Sanger sequencing. For whole-genome sequencing, DNA from 32 paired tumor and benign frozen prostate cancer samples was extracted by phenol-chloroform and purified by the ethanol precipitation method. DNA samples were fragmented in fragmentation buffer using the Covaris Ultrasonicator system. The fragmented DNA, with an average length of 500 bp, was subjected to DNA library construction. Libraries were constructed according to Illumina's protocol with DNA samples. High-throughput shotgun sequencing was performed on the Illumina HiSeq 2000 platform. For DNA sequencing, paired-end reads with a length of 90 bp were generated. Raw DNA sequencing reads were filtered using an in-house pipeline. Clean DNA reads were processed with SAMtools to remove PCR duplicates and aligned to the hg19 human reference genome with Burrows–Wheeler aligner (see URLs).

For Sanger sequencing, DNA was extracted from all 99 cases of FFPE prostate cancer tissue using a QIAamp DNA FFPE Tissue kit. PCR was performed, and PCR products were purified using a GeneJET Extraction kit according to the manufacturer's instruction and used for Sanger sequencing. The primers used for DNA amplification were as follows: Amp-Exon6-Forward 5′-ACCCATAGCTT TGGTTTCTTCTCCC-3′; Amp-Exon6-Reverse 5′-TATCTGTTTTGGACAGG TGTTTGCG-3′; Amp-Exon7-Forward 5′-ACTCATCAGATCTGGGAACTGC-3′; Amp-Exon7-Reverse 5′-AGTTGTGGCTTTGATCTGGTT-3′. Amp-Exon6-Reverse and Amp-Exon7-Forward were also used for Sanger sequencing.

Yeast two-hybrid screen. The yeast two-hybrid screen was performed with full-length SPOP cloned in frame with the GAL4 DNA-binding domain in vector PGBKT7 (Clontech). Yeast cells were transformed with PGBKT7-SPOP and a human fetal brain cDNA library. A total of 2×10^7 independent clones were screened by growth in deficient medium and X-gal staining. Positive clones were subsequently retested in fresh yeast cells, and the identities of prey were determined with interaction sequence tags (ISTs) obtained by DNA sequencing. The reading frame was verified.

RNA interference. Nonspecific control siRNA and gene-specific siRNAs for human SPOP and BRD4 were purchased from Thermo Fisher Scientific Dharmacon. siRNA transfection of cells was performed following the manufacturer's instructions. The sequences of the siRNA oligonucleotides are as follows: siSPOP_1 5′-GGAUGAUGUAAAUGAGCAA-3′; siSPOP_2 5′- GGACAGCGACTCTGAATCT-3′; siBRD4_1 5′-GAACCUCCC UGAUUACUAU-3′; siBRD4_2 5′-AGCUGAACCUCCCUGAUUA-3′; non-specific control siRNA (siC) 5′-ACAGACUUCGGAGUACCUG-3′.

Co-immunoprecipitation. To immunoprecipitate ectopically expressed Flag-tagged proteins, transfected cells were lysed 24 h after transfection in BC100 buffer. The whole-cell lysates were immunoprecipitated with monoclonal anti-Flag antibody–conjugated M2 agarose beads (Sigma-Aldrich) at 4 °C overnight. After three washes with lysis buffer followed by two washes with BC100 buffer, the bound proteins were eluted using Flag peptide (Sigma-Aldrich) prepared in BC100 buffer for 3 h at 4 °C. The eluted protein sample was resolved by SDS–PAGE. To immunoprecipitate endogenous proteins, cells were lysed with 1× cell lysis buffer (Cell Signaling Technology), and the lysate was centrifuged. The supernatant was precleared with Protein A/G beads (Sigma-Aldrich) and incubated with the indicated antibody and Protein A/G beads at 4 °C overnight. Beads were washed five times with lysis buffer, resuspended in sample buffer and analyzed by SDS–PAGE.

Western blotting. Cell lysates or immunoprecipitates were subjected to SDS–PAGE, and proteins were transferred to nitrocellulose membranes (GE Healthcare Sciences). Membranes were blocked in Tris-buffered saline (TBS, pH 7.4) containing 5% nonfat milk and 0.1% Tween-20, washed twice in TBS containing 0.1% Tween-20 and incubated with primary antibody overnight at 4 °C followed by secondary antibody for 1 h at room temperature. Proteins of interest were visualized using the Enhanced Chemiluminescence (ECL) system (Santa Cruz Biotechnology). Densitometry analysis of protein bands was performed on Gel-Pro Analyzer software.

***In vitro* ubiquitination assays.** *In vitro* ubiquitination assays were carried out using a protocol reported previously[1]. Briefly, 2 μg of APP-BP1/Uba3, 2 μg of His-UBE2M enzymes and 5 μg of NEDD8 were incubated at 30 °C for 2 h in the presence of ATP. The thioester-loaded His-UBE2M–NEDD8 was further incubated with 3 μg of His-DCNL2 and 6 μg of CUL3–RBX1 at 4 °C for 2 h to obtain neddylated CUL3–RBX1. The neddylated CUL3–RBX1, 5 μg of GST-SPOP, 5 μg of ubiquitin, 500 ng of E1 enzyme, 750 ng of E2 enzyme (UbcH5a and UbcH5b) and 5 μg of His-BRD4-N (amino acids 1–500) were incubated with 0.6 μl of 100 mM ATP, 1.5 μl of 20 μM ubiquitin aldehyde, 3 μl of 10× ubiquitin reaction buffer (500 mM Tris-HCl (pH 7.5), 50 mM KCl, 50 mM NaF, 50 mM $MgCl_2$ and 5 mM DTT), 3 μl of 10× energy regeneration mix (200 mM creatine phosphate and 2 μg/μl creatine phosphokinase) and 3 μl of 10× protease inhibitor cocktail at 30 °C for 2 h, followed by western blot analysis. Ubiquitin, E1, E2 and CUL3–RBX1 were purchased from Ubiquigent.

***In vivo* ubiquitination assays.** For the *in vivo* ubiquitination assays, C4-2 cells were transfected with plasmids for HA-ubiquitin, Flag-BRD4 and other indicated proteins. Cells were treated with 20 μM MG-132 for 8 h before they were harvested and lysed with lysis buffer (50 mM Tris-HCl, pH 7.5; 150 mM NaCl; 1% NP-40; 0.5% sodium deoxycholate; 1× protease inhibitor cocktail). The lysate was subjected to co-IP using anti-Flag antibody–conjugated agarose beads as described above.

qRT–PCR. Total RNA was isolated from transiently transfected cells using TRIzol reagent (Thermo Fisher Scientific), and cDNA was reverse-transcribed using the Superscript RT kit (Toyobo, according to the manufacturer's instructions. PCR amplification was performed using the SYBR Green PCR Mastermix Kit (Toyobo). All quantifications were normalized to the level of endogenous control GAPDH. The primer sequences for the SYBR Green qPCR used are as follows: BRD2-F 5′-CTACGTAAGAAACCCCGGAAG-3′; BRD2-R 5′-GCTTTTTCTCCAAAGCCAGTT-3′; BRD3-F 5′-CCTCAGGGAG ATGCTATCCA-3′; BRD3-R 5′-ATGTCGTGGTAGTCGTGCAG-3′; BRD4-F 5′-AG CAGCAACAGCAATGTGAG-3′; BRD4-F 5′-GCTTGCACTTGT CCTCTTCC-3′; RAC1-F 5′-TGGCTAAGGAGATTGGTGCT-3′; RAC1-R 5′-GCAAAG CGTACAAAGGTTCC-3′; FDFT1-F 5′-ACTATGTTGCTGGGCTGGTC-3′; FDF T1-R 5′-ACCTGCTCCAAACCTCTTGA-3′; DHCR24-F 5′-CAAAGG AAATGAGGCAGAGC-3′; DHCR24-R 5′-TGTGGTACAAGGAGCCATCA-3′; DHCR7-F 5′-TGACATCTGCCATGACCACT-3′; DHCR7-R 5′-ACAGGT CCTTCTGGTGGTTG-3′; MVD-F 5′-AGGACAGCAACCAGTTCCAC-3′; MVD-R 5′-CACACAGCAGCCACAAACTC-3′; PSA-F 5′-GGCAGC ATTGAACCAGAGGAG-3′; PSA-R 5′-GCATGAACTTGGTCACCTTCTG-3′; TMPRSS2-F 5′-CCTGCAAGGACATGGGTAT-3′; TMPRSS2-R 5′-CGGCACTTGTGTTCAGTTTC-3′; MYC-F 5′-GGATTCTCTGCTCTCC TC-3′; MYC-R 5′-CTTGTTCCTCCTCAGAGTC-3′; AR-F 5′-GACGCTTCTAC CAGCTCACC-3′; AR-R 5′-GCTTCACTGGGTGTGGAAAT-3′; GAPDH-F 5′-TGCACCACCAACTGCT TAGC-3′; GAPDH-R 5′-GGCATGGAC TGTGGTCATGAG-3′.

Cell proliferation assays. The CellTiter 96 AQueous One Solution Cell Proliferation Assay (MTS) (Promega) was used to measure cell growth according to the manufacturer's instructions. Briefly, cells were plated in 96-well plates at a density of 2,000 cells per well. At the indicated times, 20 μl of CellTiter 96R Aqueous One Solution Reagent was added to the medium. After incubating for 1 h at 37 °C in a cell incubator, cell growth was measured in a microplate reader at 490 nm.

Trypan blue assays. Trypan blue assays were performed to measure cell growth according to the manufacturer's instructions. Briefly, cells were plated in six-well plates at a density of 5×10^4 to 1×10^5 cells per well. At the indicated time points, cells were trypsinized and suspended in 1 ml of 1× PBS. 100 μl of cells and 100 μl of trypan blue solution (Sigma-Aldrich) were mixed, and the number of viable cells was measured using a Bio-Rad automated cell counter.

Immunohistochemistry. FFPE tumor samples from patients or C4-2 xenograft tumors were deparaffinized, rehydrated and subjected to heat-mediated antigen retrieval. The UltraSensitive S-P (Rabbit) IHC Kit (KIT-9706, Fuzhou Maixin Biotech) was used following the manufacturer's instructions with minor modifications, as reported previously[36]. Briefly, sections were incubated with 3% H_2O_2 for 15 min at room temperature to quench endogenous peroxidase activity. After antigen retrieval using unmasking solution (Vector Labs), slides were blocked with normal goat serum for 1 h and then incubated with primary antibody at 4 °C overnight. IHC analysis of tumor samples was performed using primary antibodies against BRD2 (dilution 1:250; Abcam, ab139690), BRD3 (dilution 1:200; Bethyl, A302-368A) and BRD4 (dilution 1:500; Bethyl, A301-985A100). The sections were then washed three times in 1× PBS and treated for 30 min with biotinylated goat-anti–rabbit IgG secondary antibodies (Fuzhou Maixin Biotech). After washing three times in 1× PBS, sections were incubated with streptavidin-conjugated HRP (Fuzhou Maixin Biotech). After washing three times in 1× PBS for 5 min each, specific detection was developed with 3,3′-diaminobenzidine (DAB-2031, Fuzhou Maixin Biotech). Images were acquired using an Olympus camera and matched software. IHC staining was scored by two independent pathologists on the basis of the 'most common' criteria.

RNA extraction from FFPE patient tissues and RT–qPCR. Experiments were performed using the method described previously[14,37,38]. Briefly, a 4-μm precut H&E-stained section was obtained and reviewed by a pathologist. Only blocks with ≥80% tumor cells were used. Total RNA was isolated from FFPE tissue sections from the same cohorts of subjects using the RNeasy FFPE Kit (Qiagen, 73504) using the method reported previously[39]. The NanoDrop 2000 spectrophotometer (Thermo Fisher Scientific) was used to assess RNA yield and quality. cDNA was synthesized using the PrimeScript RT reagent Kit (Perfect Real Time) according to the manufacturer's instructions (Takara, RR037A) with minor modifications. qPCR was performed using SYBR Premix Ex Taq II (Tli RNase H Plus) (Takara, RR820A) on a StepOnePlus real-time PCR system (Thermo Fisher Scientific) according to Takara's recommended cycling conditions (95 °C for 30 s, followed by 40 cycles of 95 °C for 5 s, 60 °C for 30 s and a melt curve analysis). 18S RNA served as an internal reference as reported previously[40]. The primers used in RT–qPCR are listed in **Supplementary Table 6**. All of the samples were run in triplicate on the same plate, and the expression levels of *BRD2*, *BRD3* and *BRD4* mRNAs were automatically calculated by the StepOnePlus real-time PCR system (Thermo Fisher Scientific). Comparison of the expression levels of *BRD2*, *BRD3* and *BRD4* mRNAs was performed with Mann–Whitney tests by MedCalc statistical software v10.4.7.0 (MedCalc Software bvba). A two-sided P value <0.05 was considered statistically significant.

RNA-seq and data analysis. C4-2 cells infected with lentivirus expressing empty vector (EV), HA-SPOP-F133V or BET proteins were treated with or without JQ1 (1 μM) for 24 h. Total RNA was isolated from cells using methods described previously[41]. Briefly, RNA was isolated using the RNeasy Plus Mini Kit (Qiagen). High-quality (Agilent Bioanalyzer RIN > 7.0) total RNA was employed for the preparation of sequencing libraries using the Illumina TruSeq Stranded Total RNA/Ribo-Zero Sample Prep Kit. A total of 500–1,000 ng of riboRNA-depleted total RNA was fragmented by RNase III treatment at 37 °C for 10–18 min, and RNase III was inactivated at 65 °C for 10 min. Size selection (50- to 150-bp fragments) was performed using the FlashPAGE denaturing PAGE-fractionator (Thermo Fisher Scientific) before ethanol precipitation overnight. The resulting RNA was directionally ligated, reverse-transcribed and treated with RNase H.

doi:10.1038/nm.4379

Samples with biological triplicates were sequenced using the Illumina HiSeq 2000 platform at the Mayo Clinic Medical Genome Facility. Preanalysis quality control was performed using FastQC (http://www.bioinformatics.babraham.ac.uk/projects/fastqc/) and RSeQC software[42] to ensure that raw data were in excellent condition and suitable for downstream analyses. Paired-end raw reads were aligned to the human reference genome (GRCh37/hg19) using TopHat[43]. Genome-wide coverage signals were represented in BigWig format to facilitate convenient visualization using the UCSC Genome Browser. Gene expression was measured using RPKM (reads per kilobase exon per million mapped reads) as described previously[44]. EdgeR[45] was used to identify genes that were differentially expressed between EV-expressing and SPOP-F133V-expressing C4-2 cells treated with or without JQ1.

Chromatin immunoprecipitation sequencing and data analysis and ChIP–qPCR. ChIP was performed as described previously[46]. ChIP–seq libraries were prepared using methods described previously[46], and high-throughput sequencing was performed using the Illumina HiSeq 2000 platform at the Mayo Clinic Medical Genome Facility. Data were analyzed using the following pipeline: ChIP–seq raw reads were aligned to the human reference genome (GRCh37/hg19) using Bowtie2 (2.2.9), reads mapped to one or two locations were kept for further analysis and peak calling was performed by MACS2 (2.1.1) with a *P*-value threshold of 1×10^{-5}. BigWig files were generated for visualization with the UCSC Genome Browser or Integrative Genomics Viewer (IGV). We used GREAT (see URLs) to assign peaks to their potential target genes (a peak–gene association was determined if the peak fell into a 2-kb region centered on the transcription start site of the gene). The common BRD4 target genes induced by SPOP-F133V and HA-BRD4 expression were determined independently in each of two biological repeat experiments.

For ChIP–qPCR experiments, DNA pulled down by antibodies or nonspecific IgG was amplified by real-time PCR. The ChIP primers used were as follows: RAC1 ChIP-F 5′-CCAAAGTGTTGGGATTACGG-3′; RAC1 ChIP-R 5′-CGGAGTT TCTC TGGACTTCG-3′; FDFT1 ChIP-F 5′-ACATCACATGAAGG CCGTTT-3′; FDFT1 ChIP-R 5′-GACCTTCCACCAACCACCTA-3′; DHCR24 ChIP-F 5′-CCCTGAG TCAGTCACCCTTT-3′; DHCR24 ChIP-R 5′-ACAATGGAGCTCACCACTCC-3′; DHCR7 ChIP-F 5′-GCACATTGATGGA GCGTATG-3′; DHCR7 ChIP-R 5′-TAA TAAGCAGGCCACCCAGA-3′; MVD ChIP-F 5′-CGCATTACCTCTCAGCCAAT-3′; MVD ChIP-R 5′-AGACAGGT AGCCCCCACAG-3′; PSA promoter ChIP-F 5′-CCCTCCCCTTC CACAGC-3′; PSA promoter ChIP-R 5′-GCCCTATAAAACCTTCATT CCCCAGG-3′; TMPRSS2 ChIP-F 5′-CGCCCCAGAGTCCCTTAT-3′; TMPRSS2 ChIP-R 5′-TAATCTCAGGAGGCGGTGTC-3′; MYC ChIP-F 5′-AGGGATCGCGCTGAGTATAA-3′; MYC ChIP-R 5′-TGCCTCT CGCTGGAATTACT-3′; AR ChIP-F 5′-GCAGGAGCTATTCAGGAAGC-3′; AR ChIP-R 5′-AGGTGGAGAGCAAATGCAAC-3′. Detailed information regarding PCR primers at the enhancers and promoters of all analyzed genes are also summarized in **Supplementary Table 6**.

Meta-analysis of publically available BRD4 and histone mark ChIP–seq data. BRD4 ChIP–seq data in 293T and HeLa cells (accession number GSE51633)[47], H2171 and U87 cells (accession number GSE44931)[18] and mouse acute myeloid leukemia (AML) cells (accession number GSE66122)[19] as well as H3K4me1 and H3K4me3 ChIP–seq data in LNCaP cells[33] were downloaded from the NCBI Gene Expression Omnibus. If the original alignments were based on hg18/GRCh36, they were converted into hg19/GRCh37-based alignments using CrossMap[48]. Peak calling was performed using MACS2 (v2.0.10)[49].

Analysis of JQ1-resistant gene expression in the TCGA data set and pathway analysis. Primary tumor samples from the prostate cancer cohort in TCGA have been classified into SPOP-MUT (with mutation; $n = 48$) and SPOP-WT (without mutation; $n = 449$) groups according to the mutation status of *SPOP*. Differential expression between these two groups for the JQ1-resistance-associated genes ($n = 1{,}017$) was investigated by Mann–Whitney test with the significance threshold set at $P < 0.001$. A total of 129 genes have been identified as upregulated in SPOP-MUT samples. The heat map was generated using *Z*-score-transformed expression of each gene across all samples. Pathway analyses were performed using Ingenuity IPA.

Cholesterol analysis. Cells were washed with PBS twice and lysed in lysis buffer (10 mM Tris-HCl (pH 7.6), 500 mM NaCl, 1% Triton X-100, 10 mM β-methylphenethylamine, 2 mM Na_3VO_4 and 1 mM PMSF) for 30 min on ice. The lysates were extracted in chloroform-methanol-HCl solution as described previously[50]. Cholesterol concentration was measured using Infinity reagent (Thermo Fisher Scientific).

Generation and treatment of prostate cancer xenografts in mice. Six-week-old NOD-SCID IL-2 receptor γ–null (NSG) mice were generated in house and randomly divided into different experimental groups as indicated. The animal study was approved by the Institutional Animal Care and Use Committee (IACUC) at the Mayo Clinic. All mice were housed in standard conditions with a 12-h light/12-h dark cycle and access to food and water *ad libitum*. For BET protein knockdown studies, C4-2 cells (5×10^6), infected with lentivirus expressing empty vector (EV) or HA-SPOP-F133V in combination with control shRNA or BRD2-, BRD3- or BRD4-specific shRNA were mixed with Matrigel (in 100 µl of 1× PBS plus 100 µl of Matrigel (BD Biosciences)) and injected subcutaneously into the right flank of mice. After xenografts reached a size of approximately 100 mm^3, vehicle (10% β-cyclodextrin) or JQ1 (Sigma-Aldrich) at 50 mg per kg bodyweight was administered by intraperitoneal injection 5 d per week. For studies with tumors treated with JQ1 and the AKT inhibitor GDC-0068, C4-2 cells (5×10^6) infected with lentivirus expressing empty vector (EV) or HA-SPOP-F133V were mixed with Matrigel (in 100 µl of 1× PBS plus 100 µl of Matrigel (BD Biosciences)) and injected subcutaneously into the right flank of mice. After xenografts reached a size of approximately 100 mm^3, vehicle (10% β-cyclodextrin), JQ1 (50 mg per kg bodyweight) and GDC-0068 (100 mg per kg bodyweight) were administrated individually or in combination 5 d per week. Growth in tumor volume was measured in a blinded fashion using digital calipers, and tumor volumes were estimated using the formula $(L \times W^2)/2$, where L is the length of the tumor and W is the width. Tumor volumes were compared, and P values were determined by a two-tailed Student's t-test. Upon completion of treatment, tumor grafts were dissected. Tumor tissues were divided, and a portion was subjected to formalin fixation and embedding in paraffin while the rest was frozen for protein and RNA extraction.

Statistical analysis. All data are shown as mean values ± s.d. for experiments performed with at least three replicates. Difference between two groups were analyzed using paired Student's t-tests unless otherwise specified. A P value <0.05 was considered statistically significant.

A **Life Sciences Reporting Summary** for this paper is available.

Data availability. The whole-genome sequencing data have been deposited in the European Genome-phenome Archive with accession code EGAS00001000888. RNA-seq and ChIP–seq data are available at the NCBI Gene Expression Omnibus data repository with accession code GSE88872. Uncropped western blots, along with molecular weight standards, are included in **Supplementary Figures 11–14**.

34. Hayward, S.W. *et al.* Establishment and characterization of an immortalized but non-transformed human prostate epithelial cell line: BPH-1. *In Vitro Cell. Dev. Biol. Anim.* **31**, 14–24 (1995).
35. Drost, J. *et al.* Organoid culture systems for prostate epithelial and cancer tissue. *Nat. Protoc.* **11**, 347–358 (2016).
36. Patel, A.J. *et al.* BET bromodomain inhibition triggers apoptosis of NF1-associated malignant peripheral nerve sheath tumors through Bim induction. *Cell Rep.* **6**, 81–92 (2014).
37. Renwick, N. *et al.* Multicolor microRNA FISH effectively differentiates tumor types. *J. Clin. Invest.* **123**, 2694–2702 (2013).
38. Zhao, Y. *et al.* Activation of P-TEFb by androgen receptor–regulated enhancer RNAs in castration-resistant prostate cancer. *Cell Rep.* **15**, 599–610 (2016).
39. Mittempergher, L. *et al.* Gene expression profiles from formalin fixed paraffin embedded breast cancer tissue are largely comparable to fresh frozen matched tissue. *PLoS One* **6**, e17163 (2011).
40. Hagen, R.M., Rhodes, A., Oxley, J. & Ladomery, M.R. A M-MLV reverse transcriptase with reduced RNaseH activity allows greater sensitivity of gene expression detection in formalin fixed and paraffin embedded prostate cancer samples. *Exp. Mol. Pathol.* **95**, 98–104 (2013).

41. Wang, L. *et al.* BRCA1 is a negative modulator of the PRC2 complex. *EMBO J.* **32**, 1584–1597 (2013).
42. Wang, L., Wang, S. & Li, W. RSeQC: quality control of RNA-seq experiments. *Bioinformatics* **28**, 2184–2185 (2012).
43. Trapnell, C., Pachter, L. & Salzberg, S.L. TopHat: discovering splice junctions with RNA-seq. *Bioinformatics* **25**, 1105–1111 (2009).
44. Mortazavi, A., Williams, B.A., McCue, K., Schaeffer, L. & Wold, B. Mapping and quantifying mammalian transcriptomes by RNA-Seq. *Nat. Methods* **5**, 621–628 (2008).
45. Robinson, M.D. & Oshlack, A. A scaling normalization method for differential expression analysis of RNA-seq data. *Genome Biol.* **11**, R25 (2010).
46. Boyer, L.A. *et al.* Core transcriptional regulatory circuitry in human embryonic stem cells. *Cell* **122**, 947–956 (2005).
47. Liu, W. *et al.* Brd4 and JMJD6-associated anti-pause enhancers in regulation of transcriptional pause release. *Cell* **155**, 1581–1595 (2013).
48. Zhao, H. *et al.* CrossMap: a versatile tool for coordinate conversion between genome assemblies. *Bioinformatics* **30**, 1006–1007 (2014).
49. Zhang, Y. *et al.* Model-based analysis of ChIP-Seq (MACS). *Genome Biol.* **9**, R137 (2008).
50. Zhuang, L., Kim, J., Adam, R.M., Solomon, K.R. & Freeman, M.R. Cholesterol targeting alters lipid raft composition and cell survival in prostate cancer cells and xenografts. *J. Clin. Invest.* **115**, 959–968 (2005).

doi:10.1038/nm.4379

nature research

Corresponding author(s): Haojie Huang

☐ Initial submission ☐ Revised version ☒ Final submission

Life Sciences Reporting Summary

Nature Research wishes to improve the reproducibility of the work that we publish. This form is intended for publication with all accepted life science papers and provides structure for consistency and transparency in reporting. Every life science submission will use this form; some list items might not apply to an individual manuscript, but all fields must be completed for clarity.

For further information on the points included in this form, see Reporting Life Sciences Research. For further information on Nature Research policies, including our data availability policy, see Authors & Referees and the Editorial Policy Checklist.

Experimental design

1. Sample size

Describe how sample size was determined.	Sample size was chosen based on similar studies performed in our lab and those reported in the literature. The sample size and the power to detect the differences between experimental groups have been provided on Figure 3e and in the legends of Figure 4 in the main text, and in the legends of Supplemental Figure 3 and the Statistical Analysis section in Online Methods.

2. Data exclusions

Describe any data exclusions.	No animals were excluded from the analysis.

3. Replication

Describe whether the experimental findings were reliably reproduced.	All data shown were performed with at least three technical replicates, except animal and MTS assay. MTS assay were performed with at least six technical replicates. Animal were performed with at least six independent animals for one group.

4. Randomization

Describe how samples/organisms/participants were allocated into experimental groups.	This information is provided in the section of "Generation and treatment of prostate cancer xenografts in mice" in Online Methods.

5. Blinding

Describe whether the investigators were blinded to group allocation during data collection and/or analysis.	We have stated in the section of "Generation and treatment of prostate cancer xenografts in mice" in Online Methods that growth in tumor volume was measured in a blinded fashion using digital caliper .

Note: all studies involving animals and/or human research participants must disclose whether blinding and randomization were used.

Nature Medicine: doi:10.1038/nm.4379

6. Statistical parameters

For all figures and tables that use statistical methods, confirm that the following items are present in relevant figure legends (or in the Methods section if additional space is needed).

n/a	Confirmed
☐	☒ The exact sample size (*n*) for each experimental group/condition, given as a discrete number and unit of measurement (animals, litters, cultures, etc.)
☐	☒ A description of how samples were collected, noting whether measurements were taken from distinct samples or whether the same sample was measured repeatedly
☐	☒ A statement indicating how many times each experiment was replicated
☐	☒ The statistical test(s) used and whether they are one- or two-sided (note: only common tests should be described solely by name; more complex techniques should be described in the Methods section)
☐	☒ A description of any assumptions or corrections, such as an adjustment for multiple comparisons
☐	☒ The test results (e.g. *P* values) given as exact values whenever possible and with confidence intervals noted
☐	☒ A clear description of statistics including central tendency (e.g. median, mean) and variation (e.g. standard deviation, interquartile range)
☐	☒ Clearly defined error bars

See the web collection on statistics for biologists for further resources and guidance.

Software

Policy information about availability of computer code

7. Software

Describe the software used to analyze the data in this study.

Student's t-test were performed using the Excel. ChIP-seq raw reads were aligned to the human reference genome (GRCh37/hg19) using Bowtie2 (2.2.9), and reads mapped to one or two locations were kept for further analysis, peak calling was performed by MACS2 (2.1.1) with p-value threshold of 1e-5. For RNA-seq, Pre-analysis quality control was performed using FastQC (http://www.bioinformatics.babraham.ac.uk/projects/fastqc/) and RSeQC software to ensure that raw data are in excellent condition and suitable for downstream analyses. Pair-end raw reads were aligned to the human reference genome (GRch37/hg19) using Tophat.

For manuscripts utilizing custom algorithms or software that are central to the paper but not yet described in the published literature, software must be made available to editors and reviewers upon request. We strongly encourage code deposition in a community repository (e.g. GitHub). *Nature Methods* guidance for providing algorithms and software for publication provides further information on this topic.

Materials and reagents

Policy information about availability of materials

8. Materials availability

Indicate whether there are restrictions on availability of unique materials or if these materials are only available for distribution by a for-profit company.

MG132 and cycloheximide were purchased from Sigma-Aldrich, MLN4924, Bortezomib and MK2206 were purchased from Selleckchem. JQ1 was kindly provided by Dr. James Bradner and purchased from Sigma-Aldrich. i-BET762 (i-BET) was purchased from MedchemExpress. GDC-0068 was purchased from Calbiochem.

9. Antibodies

Describe the antibodies used and how they were validated for use in the system under study (i.e. assay and species).

The following antibodies were used: SPOP (ab137537; Abcam), SPOP (16750-1-AP; proteintech), BRD2 (A302-583A; Bethyl), BRD2 (ab139690; Abcam), BRD3 (A302-368A; Bethyl), BRD4 (ab128874; Abcam), BRD4 (A301-985A; Bethyl), Myc (9E10; Sigma-Aldrich), Myc (SC-40; Santa Cruz Biotechnology), FLAG (M2; Sigma), HA (MM5-101R; Convance), Actin (AC-74; Sigma-Aldrich), DEK (13962S; Cell Signaling Technology), ERG (SC-352; Santa Cruz Biotechnology), AR (SC-816; Santa Cruz Biotechnology), SRC-3 (611104; BD), phospho-AKT-S473 (9471; Cell Signaling Technology), phospho-AKT-T308 (9275S; Cell Signaling Technology), AKT (9272; Cell Signaling Technology), phospho-S6K-T389 (9205; Cell Signaling Technology), S6K (9202; Cell Signaling Technology), β-tubulin (T4026; Sigma-Aldrich), RAC1 (23A8; BD), FDFT1 (ab195046; Abcam), DHCR24 (ab137845; Abcam), DHCR7 (ab103296; Abcam), MVD (ab12906; Abcam), HER3 (12708S; Cell Signaling Technology), INSR (ab131238; Abcam), IGF1R (SC-9038; Santa Cruz Biotechnology), mTOR (2972, Cell Signaling Technology), Raptor (24C12, Cell Signaling Technology).

10. Eukaryotic cell lines

a. State the source of each eukaryotic cell line used.

All cell lines were from human.

b. Describe the method of cell line authentication used.

LNCaP, 22Rv1 and 293T cells were obtained from the American Type Culture Collection (ATCC). C4-2 cells were purchased from Uro Corporation (Oklahoma City, OK). BPH-1 cells were kindly provided by Dr. Simon Hayward2. 293T cells were maintained in DMEM medium with 10% FBS, while LNCaP, C4-2, 22Rv1 and BPH-1 cells were maintained in RPMI medium with 10% FBS.

c. Report whether the cell lines were tested for mycoplasma contamination.

Yes. All cell lines were tested by mycoplasma contamination.

d. If any of the cell lines used are listed in the database of commonly misidentified cell lines maintained by ICLAC, provide a scientific rationale for their use.

N/A

Animals and human research participants

Policy information about studies involving animals; when reporting animal research, follow the ARRIVE guidelines

11. Description of research animals

Provide details on animals and/or animal-derived materials used in the study.

6-week-old NOD-SCID IL-2-receptor gamma null (NSG) mice were generated in house and randomly divided into different experimental groups as indicated. The animal study was approved by the IACUC at Mayo Clinic. All mice were housed in standard conditions with a 12 h light/dark cycle and access to food and water ad libitum.

Policy information about studies involving human research participants

12. Description of human research participants

Describe the covariate-relevant population characteristics of the human research participants.

N/A

Nature Medicine: doi:10.1038/nm.4379